Globules of microparacrystals in nascent isotactic polypropylene

R. Hosemann, M. Hentschel, E. Ferracini*, A. Ferrero, S. Martelli†, F. Riva†† and M. Vittori Antisari†††**

Gruppe Parakristallforschung, c/o BAM, Berlin, West Germany

(*Received* 21 *April* 1981; *revised* 27 *August* 1981)

SAXS and TEM measurements were used in studying the morphology of nascent isotactic polypropylene (PP) polymerized with a high-yield heterogeneous Ziegler–Natta $MgCl_2$ supported catalyst. In contrast to the melt- or solution-crystallized isotactic PP cases, the SAXS datam obtained here using Kratky-camera and TEM diagrams, show the characteristic scattering of globules (~1100 Å in diameter) and a remarkably small polydispersity of 0.14. TEM observations also show sometimes the presence of smaller globular particles of about 300 Å in diameter whose amount is below the resolving power of SAXS. Due to the lack of interparticle interference, lamellae do not exist and therefore no mention of an amorphous phase is required. WAXS can be analysed as a series of overlapping reflections with paracrystalline (liquid-like) distortions at $g=5\%$. These microparacrystals (mPC's) have in accordance with the α^*-law, a mean size of $(\alpha^*/g)^2\bar{d}=60$ Å and constitute the globules. From line profile analysis one finds that their polydispersity g_N is 0.4 and this agrees well with a relation between N and g_N which is deduced theoretically for microparacrystal-ensembles in the equilibrium state. A new relation between the polydispersity g^N of microparacrystals and the size of globules is derived from TEM observations. These observations sometimes show clearly separated spherical particles whose size distribution is in the range of the SAXS results, but varies from micrograph to micrograph. The morphology of the nascent PP is greatly influenced by the distribution of the active centres on the catalyst's carrier and this excludes the regular chain-folding in a crystalline phase and the existence of larger disordered chain segments in an amorphous phase. The whole volume is therefore filled with microparacrystals.

Keywords Polypropylene; small-angle X-ray scattering; microparacrystals; Ziegler–Natta catalyst; transmission electron microscopy

INTRODUCTION

It has been well established[1-3] that the microdomains in isotactic polypropylene (PP) crystallized from solution and the melt consist of folded chain order zones, but there are relatively few reports dealing with morphology and structure of 'as polymerized' PP.

Taking into account that the organization of PP macromolecules immediately after its polymerization can be helpful in understanding, on one hand, the physico-mechanical properties of the polymer and, on the other, the mechanism of polymerization with heterogeneous Ziegler–Natta catalysts, we have investigated samples of nascent isotactic PP produced by Montedison Laboratories.

EXPERIMENTAL

Preparation of nascent PP samples

The samples were prepared in a laboratory reactor, at 65°C temperature, 6–7 atm pressure and 5 h polymerization time with a high-yield heterogeneous Ziegler–Natta $MgCl_2$ supported catalyst system. The intrinsic viscosity $[\eta]$ was 1.3 to 1.8 corresponding to a $M_w=180\,000$ to 200 000.

SAXS

PP samples (powder) were examined in Lindemann capillary tubes on a high-resolution (1200 Å) Kratky camera, with CuKα-radiation. The intensities were recorded from 0.0007 to 0.017 $Å^{-1}$ b-values ($|b|=2\sin v/\lambda$) for each point using a proportional counter with pulse discriminator. The range analysed was between 0.0011 and 0.0085 b-values. Beyond $b=0.0085$ the curve presented no more significant features. Slit smearing, air- and incoherent scattering are removed in the conventional way.

TEM

The polymer, suspended in ethanol after ultrasonic-wave treatment, was deposited on Cu grating and a slight carbon evaporation was performed. Thereafter the samples were ready for direct examination by transmission technique. The observations were carried out at 200 and 125 kV on a Joel 200 apparatus. Diffraction and dark-field experiments were also performed.

RESULTS AND DISCUSSION

SAXS

The experimental curve corrected for background scattering and slit-smearing effects[4] is reported in *Figure 1*

* Centro di Studio per la Fisica delle Macromolecole, C.N.R., Bologna, Italy
** Universita di Bologna, Via Selmi 2, Bologna, Italy
† Present address: Fritz-Haber-Institut der MPG, Berlin
†† Istituto di Tecnologia dei Polimeri e Reologia, C.N.R., Via Tojano 2, Napoli, Italy
††† C.N.E.N. Casaccia, Roma, Italy

0032-3861/82/070979-06$03.00

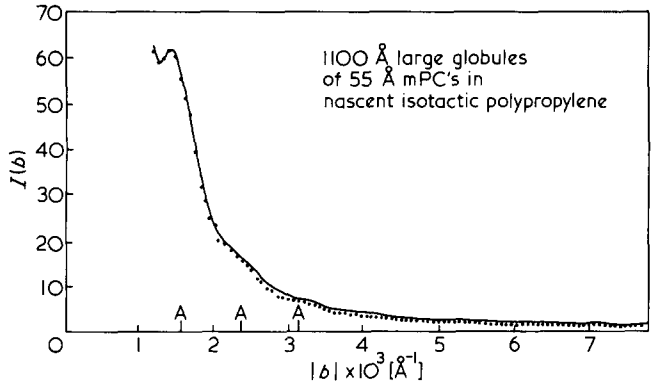

Figure 1 Observed SAXS intensity, slit smearing corrected, of isotactic nascent PP (solid line) and the calculated SAXS intensity (broken line). AAA denotes positions of the first three subsidiary maxima of a sphere with a mean diameter of 1100 Å

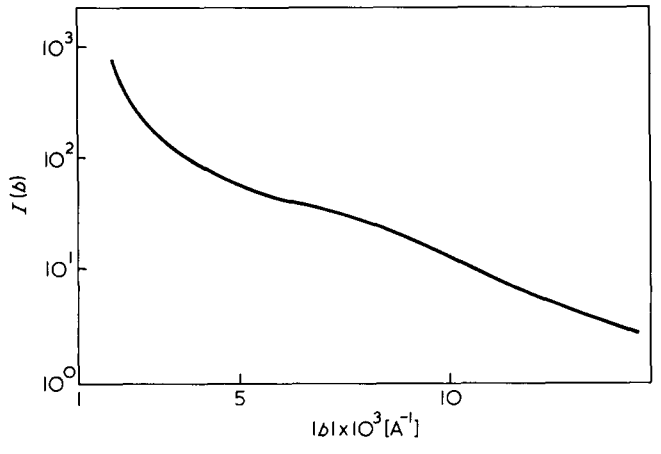

Figure 2 Observed SAXS intensity, slit smearing corrected, of isotactic nascent PP obtained by the conventional Ziegler–Natta catalyst

(solid line): The curve shows a well defined maximum at $b=0.0015$ Å^{-1} followed by broader maxima to relatively high scattering angles. This behaviour differs remarkably from that obtained by melt-crystallized samples[5] and by analogous nascent PP samples polymerized with conventional Ziegler–Natta catalysts (see *Figure 2*). In the latter case the SAXS spectrum presents a well defined, but very diffuse 'shoulder' indicating a long spacing which is a usual characteristic of the lamellar organization. Its position is correlated with the distance of the centres of lamellae within one bundle*. In order to support the assumption of no interparticle interference, even if the system is a condensed one, we introduce the following considerations:

(a) The first well defined maximum in *Figure 1* and the two broad humps following it at $b=\sim 0.0015$, 0.0025 and 0.0035 Å^{-1} b-values respectively, cannot be ascribed to higher orders of a long period reflection, but correspond to the 1st, 2nd and 3rd secondary maxima respectively of the Fourier-transform of uniform spheres of 1100 Å mean diameter approximately[6].

(b) The indistinct character of the subsidiary maxima in the small angle scattering (SAXS) indicates that the globular particles have a small polydispersity g_y defined by the weight statistical standard deviation

$$g_y=\Delta y/\bar{y} \; ; \quad \Delta_y=(\overline{y^2}-\bar{y}^2)^{1/2} \tag{1}$$

of the particle diameter y. The scattering I_1 and a small intensity component I_2 from smaller particles cannot be excluded in the SAXS of *Figure 1*. Some transmission electron micrographs (TEM) show the presence of smaller particles (about 300 Å). Therefore we use the starting solution

$$I(b)=\alpha I_1(b)+(1-\alpha)I_2(b) \; ; \quad b=\sin\nu/\lambda \tag{2}$$

The scattering intensity function of a sphere of radius R is expressed by[6]

$$I(b)\cong\left[\left(\frac{4}{3}\pi R^3\right)^2\right]\Phi(R\,b)$$

where (3)

$$\Phi(\mathrm{R\,b})=\frac{9(\sin 2\pi R\,b-2\pi R\,b\cos 2\pi R\,b)^2}{(2\pi R\,b)^6}$$

Now, if we call R_1 the radius of the larger sphere and R_2 the radius of the smaller, we use for the calculation of I_1 and I_2 (per mass unity) the following formulae:

$$I_1(b)=\sum_{i=1}^{k}(4/3)\pi {R_{1i}}^3.\ \Phi(R_{1i},b)$$

$$I_2(b)=\sum_{i=1}^{k}(4/3)\pi {R_{2i}}^3.\ \Phi(R_{2i},b) \tag{4}$$

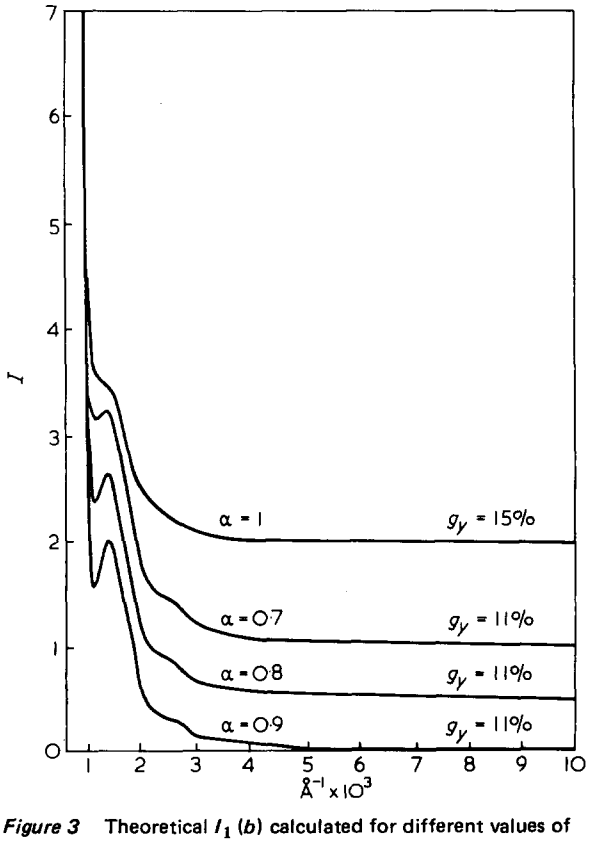

Figure 3 Theoretical I_1 (b) calculated for different values of polydispersity

* Both SAXS diagrams are made under the same conditions (sample shape, exposition time, X-ray radiation, etc.). The shoulder of *Figure 2* at 7×10^{-3} Å^{-1} is produced by interferences of lamellae which do not exist in *Figure 1*

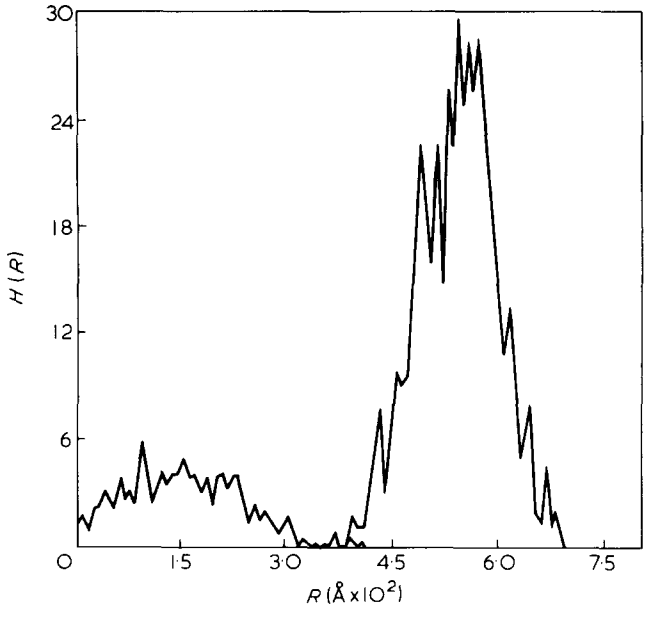

Figure 4 Histogram of particle dimension statistics: frequency *versus* radius (Å)

For computer calculations a k-value of 500 was taken and the distribution of radii dimensions (polydispersity) was initiated with two Gaussians. Introducing equations (3) and (4) to (2) and assigning suitable values to α intensity functions are calculated in arbitrary units $I(b)_{calc}$ which fit the experimental data satisfactorily, if for instance $\alpha = 0.7$ and $g_y = 11\%$ (see *Figure 1*).

Figure 4 shows a histogram of all the particle dimensions (frequency $H(R)$ *versus* particle radii R) for $\alpha = 0.7$. Larger α-values (up to 1) are also possible if g_y is given by

$$g_y = 0.11 + (\alpha - 0.7) \; ; \quad \alpha \geqslant 0.7 \tag{5}$$

As seen below, TEM observations sometimes give evidence of smaller globules with $y = 300$ Å. They cannot be excluded, but on the other hand are not evident in the SAXS. So equation (5) defines a number of possible solutions.

WAXS

Figure 5 shows the WAXS pattern. It has only a few more or less diffuse reflections and according to the conformational interpretation a strong 'diffuse background'. How can this phenomenon be explained, if, as mentioned above, in reality no amorphous phase exists? The concept of paracrystallinity gives the direct answer: Fischer *et al.*[10,12] recently showed that the WAXS of Cu-microparacrystals in a methanol catalyst can easily be synthesized by two parametrical Lorentzians

$$I(h) \sim [1 + (\pi h/\beta)]^{-z} \text{ with } h = 2d_{110} \sin \nu/\lambda \tag{6}$$

For the reflection (110) one obtains the value $z \sim 2$. This leads to a polydispersity

$$g_N = (\overline{N^2}/N^{-2} - 1)^{1/2} = \frac{1}{\sqrt{4z-4}} \sim 0.5 \tag{7}$$

which agrees well with another empirical relation combining g_N and $\bar{N}$[13] ($\bar{N}$ is calculated below).

$$g_N^2 \cong \frac{0.4}{\sqrt{N}} \tag{8}$$

The broken lines in *Figure 5* represent such profiles adapted by a DuPont 301 curve analyser. Their sum gives the intensity observed if a small background B is added* which might be caused by the grain boundaries of the microparacrystals. Here we will discuss only the relative integral widths β of the reflections. They are defined in the Appendix. For microparacrystals[9]

$$\beta = \frac{1}{N} + (\pi g h)^2 \; ; \quad g = [\overline{d^2}/\bar{d}^2 - 1]^{1/2} \tag{9}$$

(d netplane distance, N number of netplanes in a microparacrystal, h order of reflection). g defines the paracrystalline distortions within the lattice. The α^*-law[11] connects the value of N with g by

$$\sqrt{N} = \alpha^*/g \; ; \quad \alpha^* \sim 0.16 \tag{10}$$

We then obtain from equation (9)

$$\beta(h) = \frac{1}{N}\left(1 + \left(\frac{h}{2}\right)^2\right) \tag{11}$$

In *Figure 5* the numbers $1 + (h/2)^2$ together with the length of the half-width are plotted. They agree satisfactorily with the single Lorentzians. The importance of the α^*-law for colloid science and polymer physics is explained below.

The first order reflection $h = 1$ for (110) has a relative integral width $\beta \sim 1/7.5$ (*cf.* Appendix), hence $\bar{N} = 10$. Taking the value $d = 6.24$ Å of the netplane distance one

* It should be mentioned that Hindeleh *et al.* recently investigated solid state extruded isotactic PP. Its WAXS was analysed by a mixture of Gaussians and $z = 1$-Lorentzians[29]. They also found a small background B, quite similar to that in *Figure 5*

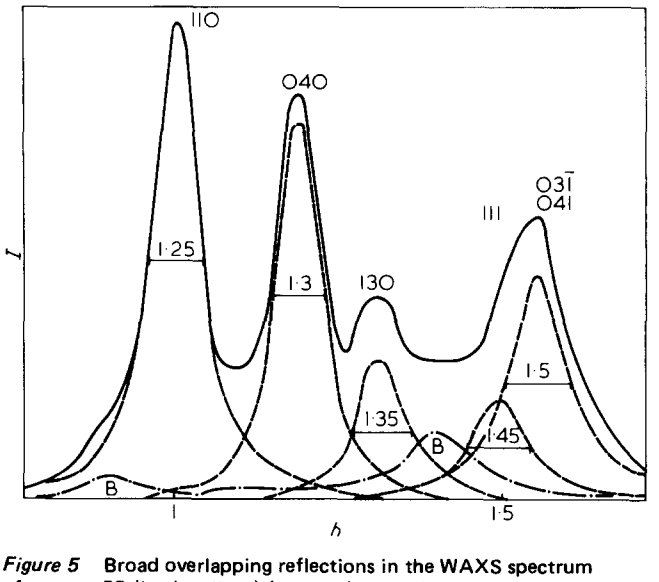

Figure 5 Broad overlapping reflections in the WAXS spectrum of nascent PP (broken lines) (see text). B is the component of the diffuse background. The numbers give the half widths $1 + (h/2)^2$ of the reflections according to equation (11)

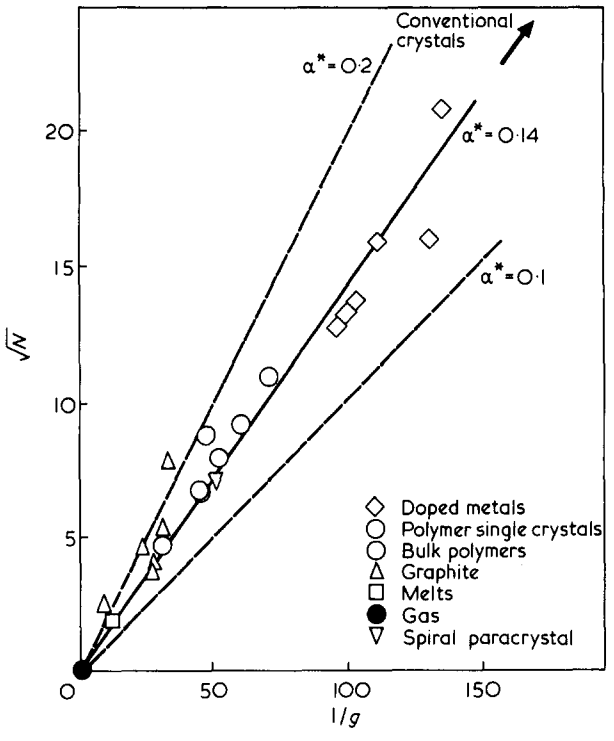

Figure 6 Graphical representation of the α*-law (equation 10). Polymers, biopolymers, catalysts, pyrolytic carbons, melts, etc. have paracrystalline lattices with liquid-like distortions which in the extreme case degenerate to the crystalline or gaseous state

obtains for the mean size of the microparacrystals $\bar{D} \sim 60$ Å.

From equation (11) one obtains for the value g in accordance with the α*-law

$$g \cong \frac{0.16}{\sqrt{N}} \sim 5\% \tag{12}$$

This value is typical for synthetic polymers with large distortions. The tails of the broad reflections create most of the 'background' in WAXS by overlapping with each other. A small remaining amount, B, may be caused by the grain boundaries as mentioned above. From equations (8) and (12) one obtains an interesting relation between g and g_N

$$g_N^2/g \sim 2.5 \tag{12a}$$

THE α*-LAW

The microparacrystals (mPC's) can be identified by their integral widths β which increase quadratically with the order, h, of the reflection (see equation (9)). If there are only two reflections $h=1$ and $h=2$ available, one should use the Warren–Averbach-method[14,15] which opens a clear distinction between line broadening by microstresses and by paracrystalline distortions[13]. In that way one obtains the values of N and g. By plotting N against g (see *Figure 6*), all microparacrystals under investigation lie in the field

$$0.1 \leqslant \alpha^* \leqslant 0.2 \tag{13}$$

The size of natural microparacrystals is unequivocally defined by the amount g of their lattice distortions (equation (7)) within the variance of equation (13). The α*-law depends to some extent on the type of chemical bonding, but its physical meaning can be easily understood. With increasing number, N, of netplanes the atoms statistically deviate more and more from the mean position by $\sqrt{N}\, g\, \bar{d}$. When this fluctuation reaches a value $\alpha^* d$, the chemical bonds are no longer flexible enough to withstand it. The 'crystallization' process is stopped and the chain segments of the other macromolecules search for other crystallization centres.

GENESIS OF GLOBULES

We assume that the growth of the globules takes place in a similar way to that of microparacrystals with the only exception that the binding forces are now the surface free energies of the microparacrystals. According to equation (8) we formulate for the number M of netplane in a globule:

$$\sqrt{M} = \beta^*/g_N \tag{14}$$

β^*, like α*, is an experimental quantity. The mean size of the globules is 1100 Å and that of the microparacrystals is 60 Å. Then we obtain, in combination with equation (7)

$$\beta^* = \sqrt{\frac{60}{1100}}\Big/0.5 = 0.46 \tag{15}$$

This means that at the surfaces of the globules, microparacrystals protude only up to a value of ~50% of their diameters. Otherwise the mPC's are forced to aggregate with other microparacrystals building up new globules. This phenomena is drawn schematically in *Figure 7*.

The value of $\alpha^* \sim 0.16$ depends on the interatomic forces in the microparacrystals. The value β^* present in macroparacrystals, however, is subject to the free energy of the mPC's which make up the macrolattice. Equation (14) may be of general importance for all colloids with globular particles of uniform sizes such as for instance latex products.

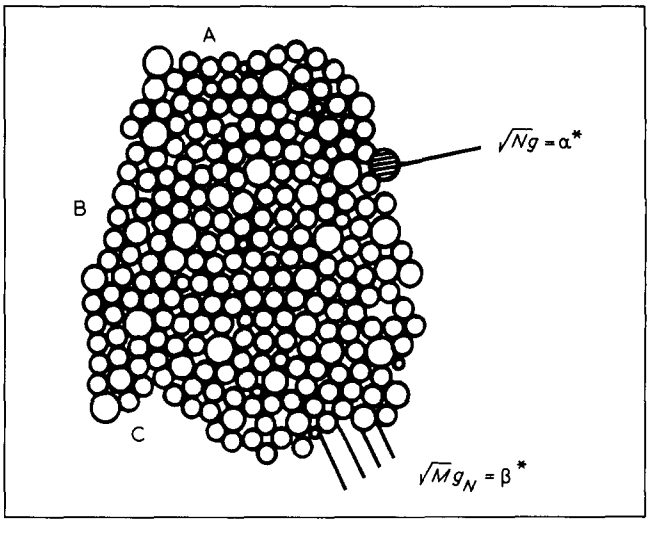

Figure 7 Microparacrystals making up a globule. A and B are the surfaces where the globules can still increase. C is the unstable part which will be disintegrated

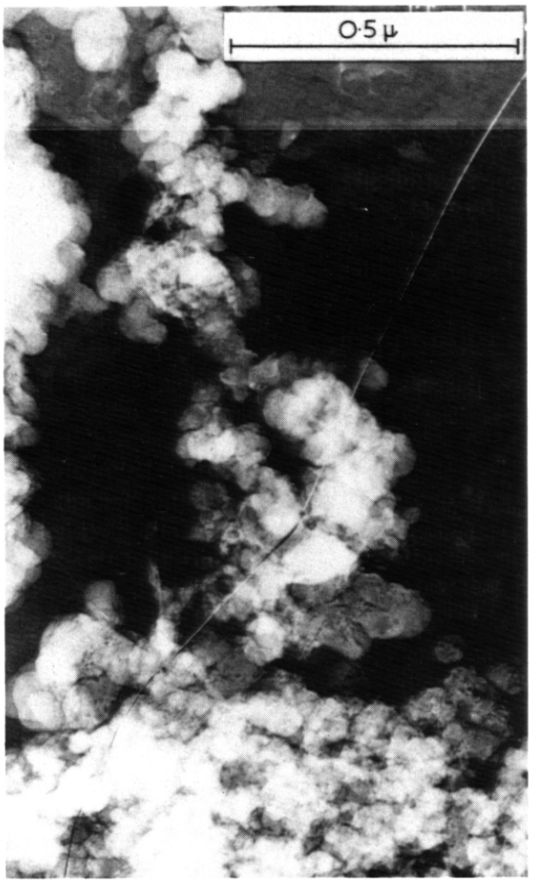

Figure 8 Transmission electron micrograph showing isolated 1000 Å globules

TEM

As mentioned above in the Experimental section, we would emphasize that the samples were examined without submitting them to severe pre-treatments which could alter the morphology of the nascent polymer.

In *Figure 8*, taken at 200 kV, we see particles between 500 and 1000 Å with evidence of 1000 Å isolated globules. They have a substructure with details about ten times smaller (or more) than the particle diameters. These details may be produced by the above mentioned 60 Å large mPC's. No 300 Å large particles exist to any extent. *Figure 9*, however, taken at lower voltage, gives evidence of mostly smaller particles (down to 200 Å in diameter) which agrees more or less with the small component I_2 of equation (2) and *Figure 4*. In *Figure 10*, again effects of the 60 Å large microparacrystals within clusters of sizes down to 150 Å are observable which again agrees with *Figure 4*. The large clouds with dimensions of 1000 Å or more may represent the larger spheres.

The TEM diagrams manifest in their own way only some of the details of the colloid structure: A quantitative evaluation of which involves an accurate counting of the particles from the TEM pictures which will be reported in a further communication.

In the dark-field micrograph of *Figure 11* spherical black particles can be observed comprising of the catalyst's support $MgCl_2$. The inorganic phase, however, does not affect the SAXS intensity (the chemical analysis reveals 70 ppm $MgCl_2$ in the sample); therefore the micrograph reveals that the catalyst's distribution is not homogeneous over the whole sample. From all the micrographs no reported evidence of catalyst entrapping

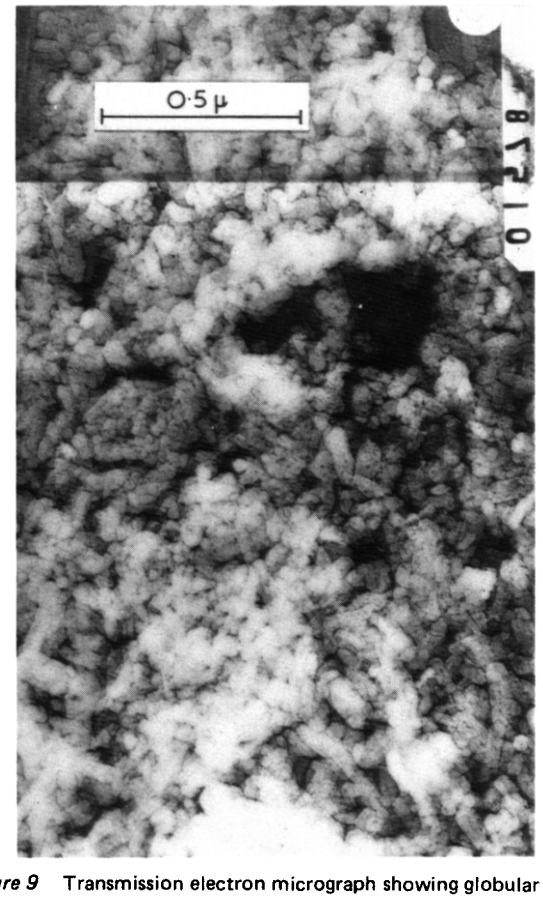

Figure 9 Transmission electron micrograph showing globular particles with wide spreading diameters down to 200 Å

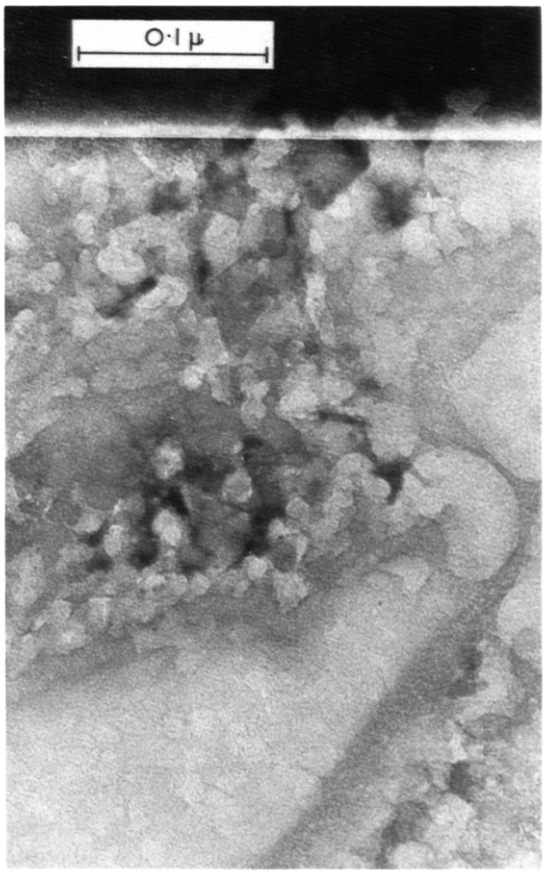

Figure 10 Transmission electron micrograph showing globular particles down to 60 Å

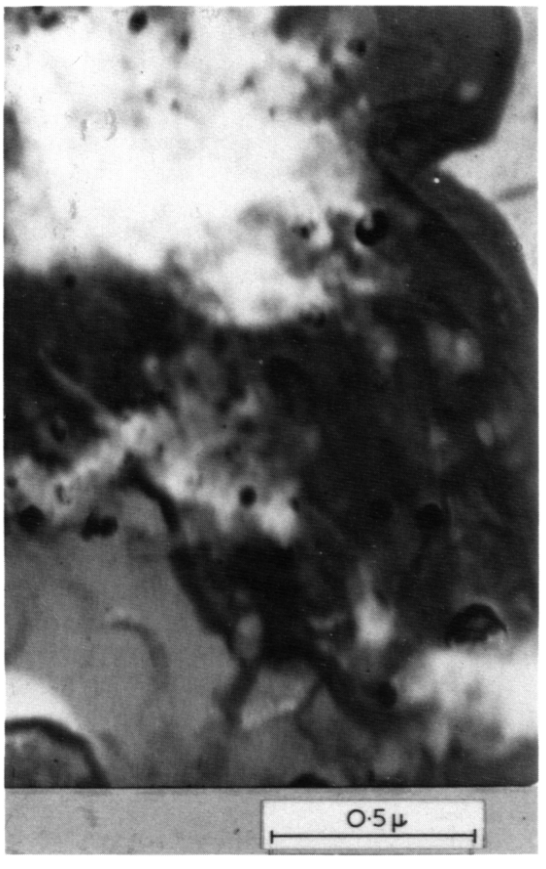

Figure 11 Dark-field of quasi-spherical particles of an inorganic crystalline component $MgCl_2$

by the polymeric phase was found.

The experimental SAXS and TEM results are in good agreement and provide useful information on the primary organisation of PP macromolecules. Blais and Manley[16] postulated the formation of fibrils at the catalyst's surface. There is no doubt that also in the present case the single chains may be produced there, but they have, as mentioned above, rather large paracrystalline distortions whereas the microfibrils cannot be observed in SAXS and WAXS diagrams.

Moreover, the polymerization was conducted at relatively low temperatures (65°C) which favours a simultaneous polymerization and crystallization mechanism. This fact could explain the lack of true crystallinity in the nascent PP samples.

CONCLUSIONS

The isotactic nascent PP obtained by the high-yield $MgCl_2$ supported Ziegler–Natta catalyst, presents a practically spherical colloidal structure without bundles of lamellae. Until now the spherical morphology had been observed only as a quarternary aggregation of macromolecules[17,18], the tertiary aggregation being either the fully extended chains or the regular folded chains such as fibrils, shish-kebabs and lamellae. It can be ignored that the lamellae are built up by microparacrystals. These microparacrystals can clearly aggregate also as globules. This fact may be explained by considering the high polymerization rate which is most probably due to the very large number of active centres in the supported catalyst system. In fact, the high dispersion of $TiCl_3$ crystals on the carrier, which has been pointed out from several authors[18,19] is supported by our experimental evidence for spherical $MgCl_2$ particles whose surface favours the most isotropic distribution of $TiCl_3$ microcrystals.

ACKNOWLEDGEMENT

The authors would like to thank Professor U. Giannini of the 'G. Donegani' Institute of Montedison, Novara (Italy) for his encouragement and helpful discussions and Mr R. Mazzocchi of Montedison for sample preparation. Professor Dr A. M. Hindeleh of the Amman University, Jordan, Professor D E. Matijevic of the Clarkson University, USA, for some helpful suggestions. Professor Dr G. Becker for contributing to our research in Berlin.

REFERENCES

1 Geil, P. H. 'Polymer Single Crystals', John Wiley (Interscience), New York, 1963
2 Mandelkern, L. 'Crystallization of Polymers', McGraw-Hill Book, London, 1964
3 Geil, P. H. *J. Polym. Sci.* 1966, **C13**, 149
4 Kortleve, G. and Vonk, C. G. *Kolloid-Z.u.Z. Polym.* 1968, **225**, 124
5 Zannetti, R., Celotti, G., Fichera, A. M., Ferrero-Martelli, A. *Eur. Polym. J.* 1968, **4**, 399
6 Guinier, A. and Fournet, G. 'Small Angle Scattering of X-Rays', John Wiley, New York, 1955
7 Joerchel, D. *Z. Naturforsch.* 1957, **12a**, 123
8 Joerchel, D. *Z. Naturforsch.* 1957, **12a**, 199
9 Hosemann, R. and Bagchi, S. N. 'Direct Analysis of Diffraction by Matter', North-Holland Publ. Comp., Amsterdam, 1962
10 Fischer, A., Dissertation, Freie Universtät Berlin, 1979
11 Baltá-Calleja, F. J. and Hosemann, R. *J. Appl. Crystallogr.* 1980, **13**, 521
12 Hosemann, R., Schmidt, W. and Fischer, A. *J. Polym. Sci., Polym. Phys. Edn.* (in press)
13 Hosemann, R., Schmidt, W., Lange, A. and Hentschel, M. *Colloid Polym. Sci.* (in press)
14 Warren, B. E. and Averbach, B. L. *J. Appl. Phys.* 1950, **21**, 595
15 Hosemann, R., Vogel, W., Weick, D. and Baltá-Calleja, F. J. *Acta Crystallogr.* 1981, **A37**, 85
16 Blais, R. and Manley, R. J. S. *J. Polym. Sci.* (A-1) 1968, **6**, 291
17 Greco, A., Perego, G., Cesari, M. and Cesca, S. *J. Appl. Polym. Sci.* 1979, **23**, 1319
18 Hock, C. W. *J. Polym. Sci.* (A-1) 1966, **4**, 3055
19 Munoz-Escalona, A. and Parada, A. *Polymer* 1979, **20**, 859
20 Hindeleh, A. M. and Yeh, G. S. Y. (in preparation)

APPENDIX

If $I_h(h)$ is the intensity function of one reflection, isolated from the others by a Lorentzian-like profile as the broken lines in *Figure 5*, then

$$\beta = \int I_h(h)\,\mathrm{d}h / I_{\max} \tag{16}$$

In the h-scale of *Figure 5* one obtains for the reflection (110)

$$\beta(1) = \int I(h)\,\mathrm{d}(h)/I(1) \sim 1/7.5 \tag{17}$$

From equation (11) one derives for the mean number of netplanes (110)

$$\bar{N} = 7.5(1+0.25) \sim 10$$

The netplane distance is $d_{110} = 6.24$ Å and the mean particle size therefore

$$\bar{D} = 62\,\text{Å}.$$